





13 **Abstract.** The development, implementation, and evaluation of a new weakly coupled ocean data  
14 assimilation (WCODA) system for the fully coupled Energy Exascale Earth System Model version 2  
15 (E3SMv2) utilizing the four-dimensional ensemble variational (4DEnVar) method are presented in this  
16 study. The 4DEnVar method, based on the dimension-reduced projection four-dimensional variational  
17 (DRP-4DVar) approach, replaces the adjoint model with the ensemble technique, thereby reducing  
18 computational demands. Monthly mean ocean temperature and salinity data from the EN4.2.1 reanalysis  
19 are integrated into the ocean component of E3SMv2 from 1950 to 2021, with the goal of providing  
20 realistic initial conditions for decadal predictions and predictability studies. The performance of the  
21 WCODA system is assessed using various metrics, including cost function reduction, root mean square  
22 error (RMSE) differences, correlation differences, and model biases. Results indicate that the WCODA  
23 system effectively assimilates the reanalysis data into the climate model, achieving consistently negative  
24 cost function reductions and notable improvements in RMSE and correlation across various ocean layers  
25 and regions. Significant enhancements are observed in the majority of global ocean regions, particularly  
26 in the North Atlantic, North Pacific and Indian Ocean. Model biases in sea surface temperature and  
27 salinity are also substantially reduced. Furthermore, analysis of the connections between the ocean states  
28 and the regional climate over the US shows that the WCODA system improves the simulation of  
29 interannual precipitation and temperature variability over the southern US. The ultimate goal of the  
30 WCODA system is to advance the predictive capabilities of E3SM for subseasonal-to-decadal climate  
31 predictions, thereby supporting research on strategic energy-sector policies and planning.



## 32 **1 Introduction**

33 Climate predictions are essential for understanding and mitigating the impacts of climate variability  
34 and change. The accuracy and reliability of climate predictions depends strongly on the initialization of  
35 the climate models, which requires realistic and high-quality initial conditions (ICs) for skillful  
36 predictions (Dirmeyer et al., 2018). Data assimilation (DA) techniques are important for providing  
37 realistic ICs by integrating observational data into the model, thereby enhancing the predictive  
38 capabilities of climate models (Tardif et al., 2014). The efficacy of DA techniques has been demonstrated  
39 through enhanced predictability on subseasonal to decadal timescales (Zhou et al., 2024).

40 Numerous studies have focused on the initialization of climate models for decadal predictions  
41 (Branstator and Teng, 2012; Polkova et al., 2019). Climate models integrate multiple components,  
42 including the atmosphere, ocean, sea ice, and land. For the initialization of climate models in decadal  
43 predictions, DA methods can be categorized into uncoupled data assimilation and coupled data  
44 assimilation (CDA). In the uncoupled method, DA is performed independently within the uncoupled  
45 atmosphere, land and ocean models rather than in a coupled model. The optimal analyses from these  
46 uncoupled models are then integrated together to establish the ICs for the climate model's predictions  
47 (Yao et al., 2021). For example, some studies directly utilize existing reanalysis data to initialize climate  
48 models for decadal predictions (Yeager et al., 2012; Tian et al., 2021). Nevertheless, the uncoupled DA  
49 method may lead to imbalances between different model components, potentially inducing initial shocks  
50 and diminishing the reliability of climate predictions (Smith et al., 2015; Zhang et al., 2020). Therefore,  
51 there is a growing interest in exploring and developing CDA methods to enhance the coherence and  
52 accuracy of the ICs for climate predictions.

53 Many research groups and institutions are actively engaged in the development and refinement of  
54 CDA methods. In CDA, the assimilation process is conducted directly within a coupled model. Compared  
55 to uncoupled DA, CDA provides balanced ICs that are more coordinated across multiple components of  
56 coupled models (Zhang et al., 2014). Previous studies have demonstrated that CDA enhances interannual  
57 climate predictions more effectively than uncoupled DA (Zhang et al., 2005; Shi et al., 2022). CDA  
58 techniques are divided into weakly coupled data assimilation (WCDA) and strongly coupled data  
59 assimilation (SCDA). In the WCDA system, reanalysis data is assimilated independently within each



60 component of the coupled model. However, through the coupled model integration, reanalysis  
61 information from one component is transmitted to other components through interactions across multiple  
62 systems (Browne et al., 2019; He et al., 2020). Sequential DA is distinctly partitioned into two primary  
63 stages: the analysis and forecast steps. During the WCDA analysis step, reanalysis information from one  
64 component can not directly influence other components due to the lack of cross-component background  
65 error covariances. Nonetheless, the coupled model is employed during the forecast step to transfer  
66 reanalysis information from single component to others through the integration of the coupled system  
67 (Laloyaux et al., 2016; Carrassi et al., 2018). The primary distinction between WCDA and uncoupled  
68 DA is the use of the coupled model during the forecast step (Zhang et al., 2020). Recent studies have  
69 developed WCDA systems that separately assimilate reanalysis data from the atmosphere (Li et al., 2021),  
70 land (Shi et al., 2024), and ocean (He et al., 2017) into coupled models. On the other hand, SCDA  
71 employs cross-component background error covariances during the analysis step to directly exert an  
72 instantaneous impact of reanalysis information from single component on the state variables of other  
73 components, treating all Earth system components as an integrated whole (Sluka et al., 2016). Moreover,  
74 SCDA also allows reanalysis information from single component to propagate to other components  
75 during the forecast step through the coupled model integration (Yoshida and Kalnay, 2018). Therefore,  
76 SCDA offers potential benefits, including reduced model drift and enhanced forecast accuracy (Smith et  
77 al., 2015). Nevertheless, the development of SCDA presents considerable obstacles, primarily due to the  
78 complexity of accurately establishing cross-component background error covariances (Penny and Hamill,  
79 2017). As a result, most existing CDA systems continue to employ the WCDA systems.

80 This study presents the development and implementation of the weakly coupled ocean data  
81 assimilation (WCODA) system for the fully coupled Energy Exascale Earth System Model version 2  
82 (E3SMv2), utilizing the four-dimensional ensemble variational (4DEnVar) method. The 4DEnVar  
83 method is based on the dimension-reduced projection four-dimensional variational (DRP-4DVar)  
84 approach, notable for its innovative application of 4DVar by replacing the adjoint model with the  
85 ensemble approach (Wang et al., 2010). In the WCODA system, monthly mean ocean temperature and  
86 salinity data from the EN4.2.1 reanalysis are incorporated into the ocean component of E3SMv2 to  
87 provide realistic ICs for decadal predictions. Although the assimilation process during the analysis step





88 is conducted independently within the ocean component, the fully coupled E3SMv2 model is employed  
89 during the forecast step to transmit reanalysis information from the ocean to other components (e.g.,  
90 atmosphere and land) through multi-component interactions. Consequently, the reanalysis information  
91 assimilated into the ocean ICs affects other model components through the integration of the fully  
92 coupled model, emphasizing the operation of this system as a WCDA system. The primary objective of  
93 this WCODA system is to advance our understanding of the ocean's role in climate predictability. Shi et  
94 al. (2024) implemented a weakly coupled land data assimilation in E3SMv2 for isolating the land's role  
95 in climate predictability. By improving the accuracy of ICs for both land and ocean, we aim to advance  
96 the predictive capabilities of E3SM for decadal predictions, ultimately supporting research on energy-  
97 sector policy and planning.

98 This study presents and evaluates the 4DEnVar-based WCODA system for E3SMv2. Section 2  
99 provides a detailed description of the E3SMv2 model, the ocean reanalysis data, and the framework of  
100 implementing the 4DEnVar-based WCODA system. Section 3 evaluates the assimilation performance of  
101 the WCODA system. Finally, Section 4 provides the conclusions.

102

## 103 **2 Methodology**

### 104 **2.1 E3SM Overview**

105 Developed by the U.S. Department of Energy, the Energy Exascale Earth System Model version 2  
106 (E3SMv2) is a state-of-the-art climate model to advance our understanding of climate variability and its  
107 future changes (Leung et al., 2020). E3SMv2 integrates multiple components to simulate the complex  
108 interactions within the climate system, encompassing the atmospheric, sea ice, ocean, land, and river  
109 transport components. The atmospheric component (EAMv2) employs sophisticated representations of  
110 turbulence, clouds, and aerosol processes (Zhang et al., 2023) and features a nonhydrostatic dynamical  
111 core (Taylor et al., 2020). It operates on a dynamic grid with a horizontal resolution of approximately  
112 110 km and includes 72 vertical layers that extend to the stratosphere (Golaz et al., 2022). The sea ice  
113 component (MPAS-SI) simulates the formation, evolution, and melting of sea ice, with detailed  
114 thermodynamics and dynamics processes (Turner et al., 2022). The ocean component (MPAS-O) is  
115 responsible for modeling the physical state and biogeochemical processes of the ocean, including detailed



116 simulations of ocean currents, temperature, and salinity (Reckinger et al., 2015). The land component  
117 (ELMv2) encompasses various land surface processes, including biophysical processes, soil processes,  
118 and surface hydrology (Golaz et al., 2019). These simulations are crucial for understanding land-  
119 atmosphere interactions and their impact on climate variability. Additionally, the river transport  
120 component (MOSARTv2) simulates the hydrological dynamics of water flow through river basins,  
121 providing insights into freshwater resources, flood risks, and sediment transport (Li et al., 2013). The  
122 CPL7 coupler dynamically integrates all five components through regulating the exchange of energy,  
123 water, and momentum fluxes between different components (Craig et al., 2012). The comprehensive  
124 evaluation of the E3SMv2 model is presented from Golaz et al. (2022).

125

## 126 **2.2 Ocean Reanalysis Dataset**

127 The ocean temperature and salinity data in this study are derived from the EN4.2.1 ocean reanalysis  
128 dataset. Produced by the Met Office Hadley Centre, the EN4.2.1 dataset integrates observations from  
129 diverse sources such as Argo floats, ship-based measurements, and satellite data (Good et al., 2013).  
130 These observations undergo rigorous quality control procedures to ensure the accuracy and reliability of  
131 the EN4.2.1 reanalysis (Chen et al., 2020). The comprehensive coverage and high resolution of the  
132 EN4.2.1 reanalysis are instrumental for representing the vertical and temporal dynamics of ocean  
133 temperature and salinity. The EN4.2.1 reanalysis datasets have been extensively validated and are  
134 commonly utilized in numerous climate research (Good et al., 2013; Armour et al., 2016).

135 To initialize decadal climate predictions, monthly mean ocean temperature and salinity data from  
136 the EN4.2.1 reanalysis are assimilated into the fully coupled E3SMv2 model across sixty ocean layers  
137 from 1950 to 2021. The choice to utilize monthly mean reanalysis data is based on two primary reasons:  
138 Firstly, data with higher temporal resolution (less than one month) might produce unwanted noise,  
139 potentially compromising the accuracy of decadal predictions. Secondly, the initialization for decadal  
140 predictions requires assimilation cycles spanning several decades, and assimilating complex, real-time  
141 observations over such extended periods would be computationally prohibitive. Therefore, in line with  
142 most existing studies that use reanalysis data for initializing decadal predictions (Pohlmann et al., 2019;  
143 Tian et al., 2021), this study assimilates the monthly mean EN4.2.1 reanalysis through the WCODA



144 system for decadal predictions.

145

### 146 **2.3 Implementation of the 4D<sub>En</sub>Var-based WCODA System**

147 The 4D<sub>En</sub>Var method employed by the WCODA system is derived from the DRP-4DVar  
148 assimilation approach. The DRP-4DVar technique addresses the high computational demands of  
149 traditional 4DVar by employing an ensemble approach rather than utilizing the adjoint model,  
150 significantly reducing the computational resources required for implementation (Wang et al., 2010). This  
151 advanced method enhances computational efficiency by projecting the high-dimensional state space onto  
152 a lower-dimensional subspace defined by an ensemble of historical samples. DRP-4DVar achieves an  
153 optimal solution within this sample space by aligning observations with model-generated historical time  
154 series over a four-dimensional window (Wang et al., 2010). The DRP-4DVar approach has been  
155 effectively implemented across multiple numerical models, demonstrating its accuracy and effectiveness  
156 (Zhao et al., 2012; Shi et al., 2021; Zhu et al., 2022). The comprehensive explanation of the DRP-4DVar  
157 method is provided in Wang et al. (2010). The DRP-4DVar method has also been implemented in a  
158 weakly coupled land data assimilation system in E3SMv2 (Shi et al., 2024).

159 Figure 1 illustrates the workflow of the 4D<sub>En</sub>Var-based WCODA system utilizing the DRP-4DVar  
160 approach within the fully coupled E3SMv2 model. The DRP-4DVar algorithm requires three primary  
161 inputs: observational innovation ( $\tilde{y}'_{obs}$ ), model background ( $x_b$ ), and perturbation samples. Initially, fully  
162 coupled E3SMv2 simulation is conducted for one month to generate both the model background ( $x_b$ )  
163 and observational background ( $y_b$ ). Specifically, the model background ( $x_b$ ) refers to the monthly initial  
164 condition prior to data assimilation, while the observational background ( $y_b$ ) denotes the monthly mean  
165 model states. Subsequently, the observational innovation ( $\tilde{y}'_{obs}$ ) is calculated as the difference in monthly  
166 mean ocean salinity and temperature between the EN4.2.1 reanalysis ( $y_{obs}$ ) and the monthly mean  
167 model states ( $y_b$ ). From 100 years of balanced pre-industrial control (PI-control) simulations, 30 sets of  
168 monthly mean forecast samples ( $\tilde{y}'$ ) are selected based on their highest correlations with the  
169 observational innovation. More specifically, the monthly mean forecast samples are computed by  
170 removing the long-term PI-control monthly climatology from the selected PI-control monthly mean  
171 output, which are then divided by the observational error. The observational error is computed based on



172 the statistical variance and covariance of the EN4.2.1 reanalysis. Correspondingly, 30 sets of monthly  
173 initial condition samples ( $x'$ ) for the monthly mean forecast samples are derived. The analysis increment  
174 is calculated within the perturbation samples, which consist of 30 monthly initial condition samples and  
175 their corresponding monthly mean forecast samples. Due to the limited number of samples and to  
176 diminish the influence of spurious correlations between distant grid points, a localization procedure is  
177 incorporated into the assimilation process (Wang et al., 2018). Finally, the DRP-4DVar algorithm solves  
178 for the analysis increment within the sample space, which is then added to the model background to  
179 produce the optimal analysis ( $x_a$ ).

180 Figure 2 delineates the assimilation process using the DRP-4DVar method within the 4DEnVar-  
181 based WCODA system for the fully coupled E3SMv2 model. This assimilation process includes both the  
182 analysis and forecast steps through each one-month assimilation window. In the initial stage, the fully  
183 coupled E3SMv2 model employs the model background ( $x_b$ ) as the monthly initial condition to run for  
184 one month, producing the monthly mean model outputs for ocean temperature and salinity ( $y_b^{ocn}$ ). During  
185 the analysis step, the observational innovation ( $y'_{obs}$ ) is computed by comparing the discrepancies  
186 between the EN4.2.1 reanalysis ( $y_{obs}^{ocn}$ ) and the model's monthly mean outputs ( $y_b^{ocn}$ ) for ocean  
187 temperature and salinity. The DRP-4DVar algorithm then utilizes this observational innovation and the  
188 PI-control samples to compute the optimal analysis of the ocean component ( $x_a^{ocn}$ ) at the start of the  
189 assimilation window. During the subsequent forecast step, the optimal analysis ( $x_a$ ) includes both the  
190 optimal ocean analysis ( $x_a^{ocn}$ ) and the background states of other components prior to assimilation. This  
191 optimal analysis serves as the new initial condition for the fully coupled E3SMv2 model to run for one  
192 month to generate the next month's forecast. During this fully coupled model integration, reanalysis  
193 information from the ocean component is transmitted to the other model components through interactions  
194 across multiple systems. Although the assimilation is directly applied to the ocean component, the use of  
195 the initial conditions of all components from the optimal analysis and the fully coupled climate model  
196 during the forecast step ensures that the reanalysis information from the optimal ocean analysis  
197 influences other components through interactions across multiple systems. Therefore, according to the  
198 definition of the WCDA system from previous studies (Carrassi et al., 2018; Zhou et al., 2024), this  
199 assimilation system is designated as the WCODA system. Using the same DA approach, Shi et al. (2024)



200 documented the implementation of DRP-4DVar as a weakly coupled land data assimilation system in  
201 E3SMv2.

202

## 203 2.4 Experiment Design

204 Two distinct numerical experiments are performed in this study to assess the effectiveness of ocean  
205 data assimilation within the 4DEnVar-based WCODA system. (1) The control simulation (CTRL) is a  
206 free-running fully coupled integration over a 72-year period from 1950 to 2021, driven exclusively by  
207 observed external forcings. This free-running simulation allows unrestricted interactions among the  
208 various Earth system components, including the atmosphere, land, and ocean. The CTRL simulation  
209 serves as a baseline for evaluating the assimilation effectiveness of the WCODA system. (2) The  
210 assimilation experiment (ASSIM) incorporates monthly mean ocean temperature and salinity data from  
211 the EN4.2.1 reanalysis into the ocean component of the fully coupled E3SMv2 model across sixty ocean  
212 layers. This assimilation is conducted using a one-month assimilation window, covering the same 72-  
213 year period from 1950 to 2021. At the beginning of each monthly assimilation window, the EN4.2.1  
214 reanalysis information is incorporated into the ocean state variables, after which the fully coupled model  
215 continues with free integration. During this free integration process, the reanalysis information  
216 assimilated into the ocean ICs influences other model components through interactions across multiple  
217 systems. The historical external forcings for both the ASSIM and CTRL experiments are derived from  
218 the CMIP6 protocol (Guo et al., 2020).

219

## 220 2.5 Assessment Criteria

221 To comprehensively evaluate the effectiveness of the WCODA system, multiple quantitative metrics  
222 are employed, including the root mean square error (RMSE), correlation coefficient, and cost function  
223 reduction. The reduction rate of the cost function serves as a fundamental measure to assess the  
224 assimilation system's accuracy, calculated using the formula:

$$225 \frac{\frac{1}{2}(\mathcal{Y}_{obs} - \mathcal{Y}_a)^T \mathbf{R}^{-1}(\mathcal{Y}_{obs} - \mathcal{Y}_a) - \frac{1}{2}(\mathcal{Y}_{obs} - \mathcal{Y}_b)^T \mathbf{R}^{-1}(\mathcal{Y}_{obs} - \mathcal{Y}_b)}{\frac{1}{2}(\mathcal{Y}_{obs} - \mathcal{Y}_b)^T \mathbf{R}^{-1}(\mathcal{Y}_{obs} - \mathcal{Y}_b)} \quad (1)$$

226 Here,  $\mathcal{Y}_{obs}$  denotes the EN4.2.1 reanalysis,  $\mathcal{Y}_b$  represents the pre-assimilation observational



227 background,  $y_a$  indicates the post-assimilation monthly mean model analyses, and  $\mathbf{R}$  denotes the  
228 observation error covariance matrix. Negative values of the cost function reduction signify the successful  
229 integration of reanalysis data into the model's state variables. To validate the correctness of this  
230 assimilation system, the EN4.2.1 reanalysis continues to be utilized as the reference data for evaluation.

231

### 232 **3 Results**

#### 233 **3.1 Cost Function Reduction**

234 In Figure 3, the monthly variation in the reduction rate of the cost function for the 4DEnVar-based  
235 WCODA system is presented for the 72-year period from 1950 to 2021. A negative value of the cost  
236 function reduction signifies the successful assimilation of reanalysis data into the coupled model. The  
237 cost function reduction rate reaches -12.03% in the first month. Over the entire 72-year period from 1950  
238 to 2021, the average monthly cost function reduction rate is -4.20% for all months in ASSIM. More  
239 importantly, the reduction rate of the cost function remains negative in each month of assimilation,  
240 underscoring the effectiveness and stability of the WCODA system. These findings demonstrate the  
241 successful implementation of the WCODA system, confirming that the EN4.2.1 reanalysis data have  
242 been effectively integrated into the fully coupled model.

243

#### 244 **3.2 Performance of RMSE Differences**

245 Figure 4 illustrates the RMSE differences of monthly ocean temperature between ASSIM and CTRL  
246 from 1950 to 2021 across nine ocean layers. Negative values indicate a reduction in RMSE, signifying  
247 improvements due to assimilation, while positive values denote an increase in RMSE, indicating  
248 degradations. Overall, the assimilation from the WCODA system leads to marked improvements in ocean  
249 temperature simulations across most global regions. Both upper and deeper ocean layers exhibit  
250 widespread negative RMSE differences, indicating improvements after assimilation, particularly in the  
251 tropical and mid-latitude ocean regions. Notable regions of improvement include the North Atlantic,  
252 tropical and North Pacific, Indian Ocean, and parts of the Southern Ocean. In the deeper layers, this  
253 pattern of improvements persists, though with more pronounced degradation observed in the South  
254 Atlantic and specific areas of the southern Pacific Ocean. This degradation in the deeper layers may be



255 attributed to larger observational errors in these regions or limitations in the model's ability to accurately  
256 represent deep-ocean dynamics (Wunsch and Heimbach, 2007; Balmaseda et al., 2013).

257 The RMSE differences for ocean salinity between ASSIM and CTRL across various ocean layers  
258 are presented in Figure 5. The majority of ocean regions display notable improvements for ocean salinity  
259 after assimilation, as evidenced by the prevalence of negative RMSE differences. Both upper and deeper  
260 ocean layers show relatively consistent areas of improvements. Significant enhancements are particularly  
261 evident in the North Atlantic, North Pacific, and parts of the Indian Ocean. However, certain areas exhibit  
262 degradation in RMSE. These regions are primarily located in parts of the southern Pacific Ocean. The  
263 degradation in these areas could be attributed to the inherent challenges of accurately assimilating data  
264 in regions with complex ocean dynamics or limited observational data availability (Edwards et al., 2015;  
265 Stammer et al., 2016).

266

### 267 **3.3 Performance of Correlation Differences**

268 Figure 6 illustrates the differences between ASSIM and CTRL in their correlations with observed  
269 monthly ocean temperature from 1950 to 2021 across nine ocean layers. Positive values denote an  
270 increase in correlation following assimilation, indicating improvements, whereas negative values suggest  
271 a decrease in correlation. Across the majority of global ocean regions, assimilation has generally led to  
272 significant improvements in correlation for ocean temperature simulations, with positive values in  
273 correlation differences widely distributed. The overall behavior of the upper and deeper ocean layers is  
274 largely consistent. Notably, the equatorial Pacific Ocean exhibits substantial improvements across  
275 multiple depths, indicating potential enhancements in modeling phenomena such as the El Niño-Southern  
276 Oscillation (ENSO). The North Pacific and parts of the Indian Ocean also demonstrate considerable  
277 improvements. However, certain areas exhibit diminished performance, possibly due to sparse  
278 observational data or complex ocean dynamics. In summary, ASSIM has demonstrably enhanced ocean  
279 temperature simulations by reducing RMSE (Fig. 4) and improving correlation (Fig. 6) across many  
280 ocean regions, particularly in the tropical and North Pacific, Indian Ocean, and parts of the North Atlantic.

281 The correlation differences for ocean salinity between ASSIM and CTRL across various ocean  
282 layers are depicted in Figure 7. The majority of global ocean regions exhibit marked improvements for



283 ocean salinity, with positive correlation differences dominating. These enhancements are consistently  
284 observed from the upper layers to deeper layers. Noteworthy improvements are particularly evident in  
285 the tropical and North Pacific, North Atlantic, equatorial Atlantic, and parts of the Indian Ocean.  
286 Nevertheless, some regions display a decrease in correlation, such as parts of the Southern Ocean. Overall,  
287 ASSIM has significantly improved simulations of ocean salinity in many ocean regions, as evidenced by  
288 reduced RMSE (Fig. 5) and improved correlation (Fig. 7), particularly in the North Atlantic, North  
289 Pacific, and parts of the Indian Ocean.

290

### 291 **3.4 Vertical and Temporal Analysis of RMSE and Bias for Ocean Temperature and Salinity**

292 Figure 8 presents the vertical profiles of the globally averaged RMSE variations in ocean  
293 temperature and salinity comparing ASSIM and CTRL. Negative values in the RMSE difference indicate  
294 a reduction in the global mean RMSE due to assimilation. For ocean temperature, the RMSE differences  
295 are relatively small but become more negative within the upper 85 meters of the ocean. As the depth  
296 increases beyond 135 meters, the RMSE differences become significantly negative, indicating a marked  
297 improvement in ocean temperature after assimilation. Unlike temperature, the salinity RMSE differences  
298 show substantial deviations in the upper layers, specifically within the first 155 meters of the ocean,  
299 reflecting significant improvements. However, the RMSE differences gradually decrease as depth  
300 increases, possibly due to the complexity of salt transport mechanisms in deep waters or larger  
301 observational errors in these layers (Jacobs et al., 2021; Wang et al., 2015). This suggests that the  
302 assimilation of salinity data has a more pronounced effect in the upper ocean layers compared with the  
303 deeper regions. In summary, these results emphasize the capability of the WCODA system in enhancing  
304 the simulation accuracy for both ocean temperature and salinity.

305 The temporal evolutions of the global mean bias and RMSE for vertically averaged ocean  
306 temperature and salinity are illustrated in Figure 9. The temperature bias (Fig. 9a) in CTRL is persistently  
307 positive, indicating a systematic overestimation of ocean temperature. In contrast, ASSIM consistently  
308 reduces this bias, with values approaching the zero line. Similarly, the temperature RMSE (Fig. 9b)  
309 highlights a significant decrease in RMSE for ASSIM compared to CTRL, reflecting a more accurate  
310 alignment with observed temperature. For ocean salinity, the salinity bias (Fig. 9c) reveals that CTRL





311 maintains a consistent negative bias, suggesting an underestimation of ocean salinity. However, ASSIM  
312 effectively mitigates this bias, bringing the bias values closer to the zero line. Furthermore, the salinity  
313 RMSE (Fig. 9d) is notably lower in ASSIM than CTRL, indicating enhanced model performance and a  
314 closer match to observed salinity. Overall, ASSIM exhibits superior performance relative to CTRL in  
315 reducing bias and RMSE for both ocean temperature and salinity.

316

### 317 **3.5 Climatological Mean Differences for Sea Surface Temperature and Salinity**

318 Figure 10 presents the climatological mean differences for both sea surface temperature (SST) and  
319 salinity (SSS) from 1950 to 2021. Pronounced cold biases are evident in the SST difference between  
320 CTRL and observation (Fig. 10a), particularly in the tropical and North Pacific, North Atlantic, and parts  
321 of the Indian Ocean. Significant warm biases are observed in the Southern Ocean and parts of the South  
322 Atlantic. In contrast, these SST biases found in CTRL are substantially reduced by ASSIM (Fig. 10b),  
323 especially in the North Pacific and North Atlantic, where the cold biases are diminished, and in the  
324 Southern Ocean, where the warm biases are corrected. The SSS difference between CTRL and  
325 observation highlights a global pattern of salinity biases (Fig. 10c). The CTRL simulation generally  
326 underestimates salinity across most global oceans, indicating a widespread lower salinity. This fresh bias  
327 is particularly pronounced in the North Atlantic and North Pacific. Compared with CTRL, ASSIM  
328 significantly increases the salinity estimates, thereby reducing the overall fresh biases in CTRL (Fig.  
329 10d). Notable improvements are observed in the North Atlantic, North Pacific, and parts of the Southern  
330 Ocean. In summary, ASSIM demonstrates marked improvements in both SST and SSS biases compared  
331 to CTRL, emphasizing the importance and effectiveness of the WCODA system in enhancing model  
332 accuracy and reliability.

333

### 334 **3.6 Influence of ocean data assimilation on the regional climate over land**

335 To further assess the effectiveness of the WCODA system, a preliminary analysis is conducted to  
336 examine the impact of ocean data assimilation on the regional climate over land through the weakly  
337 coupled data assimilation system. Motivated by the influence of the El Niño-Southern Oscillation and  
338 the North Atlantic Oscillation on the US regional climate (e.g., Higgins et al., 2000), we focus our



339 analysis on the simulation of interannual precipitation and temperature variability over the contiguous  
340 US. Correlations between the observed and simulated time series of detrended annual precipitation and  
341 temperature anomalies for multiple US regions show higher correlations for ASSIM compared to CTRL,  
342 although the correlations are generally low (not shown). For the southern US where statistically  
343 significant differences are found for the correlations between ASSIM and observations relative to the  
344 correlations between CTRL and observations, Fig. 11 demonstrates notable improvements in ASSIM to  
345 capture the observed interannual variability in both annual precipitation and temperature anomalies. For  
346 precipitation, the wet-dry transitions from 1982 to 1989 and from 2008 to 2016 are more accurately  
347 represented in ASSIM compared to CTRL. ASSIM also effectively reproduces the temporal evolution of  
348 temperature anomalies during the periods 1982-1993 and 2006-2013. The correlation between ASSIM  
349 and observed precipitation is 0.51, much higher than 0.02 in CTRL. Similarly, the correlation for  
350 temperature increases from -0.05 in CTRL to 0.42 in ASSIM. Both correlations for precipitation and  
351 temperature in ASSIM are statistically significant at the 95% confidence level. The enhanced simulation  
352 of interannual climate variability in ASSIM may be attributed to its improved representation of oceanic  
353 variability, particularly ENSO-related variability, which is critical for driving regional climate anomalies  
354 through air-sea interactions (Ropelewski and Halpert, 1986; McPhaden et al., 2006). Further research is  
355 needed to understand the influence of the WCODA system on improving predictability of regional  
356 climate over land.

357

#### 358 **4 Conclusions**

359 This study documents the development and assessment of the new 4DEnVar-based WCODA system  
360 in the fully coupled E3SMv2 model, employing the DRP-4DVar method. The DRP-4DVar approach  
361 significantly reduces computational demands by replacing the traditional adjoint model with the  
362 ensemble technique. As a weakly coupled assimilation system, the WCODA system independently  
363 assimilates ocean reanalysis data within the ocean component during the analysis step. However, during  
364 the subsequent forecast step, the reanalysis information from the optimal ocean analyses is propagated  
365 to other components of the Earth system through interactions across multiple systems, thereby enhancing  
366 the coherence of ICs across the climate model.



367 Monthly mean ocean temperature and salinity data from the EN4.2.1 reanalysis are integrated into  
368 the ocean component of E3SMv2 from 1950 to 2021, which can be used to provide realistic ICs for  
369 decadal climate predictions. The effectiveness of the WCODA system has been assessed using several  
370 metrics, including cost function reduction, correlation differences, RMSE differences, and model biases.  
371 The cost function reduction consistently shows negative values in each month over the 72-year period,  
372 indicating successful assimilation of the EN4.2.1 reanalysis data into the climate model. Compared to  
373 CTRL, ASSIM achieves significant reductions in RMSE and enhancements in correlation across various  
374 ocean layers and regions, with notable improvements observed in the North Atlantic, North Pacific and  
375 Indian Ocean. ASSIM substantially mitigates model biases for SST and SSS observed in CTRL,  
376 particularly reducing cold biases in the North Pacific and North Atlantic, correcting warm biases in the  
377 Southern Ocean, and significantly increasing salinity estimates to reduce the model fresh biases.  
378 Moreover, the temporal evolutions of interannual precipitation and temperature variability over the  
379 southern US are more effectively captured by ASSIM compared to CTRL through the influence of the  
380 ocean data assimilation in the coupled climate system.

381 Despite these advancements, the WCODA system exhibits limitations in certain regions,  
382 particularly in the deeper layers of the southern Pacific Ocean and South Atlantic. These challenges are  
383 likely due to sparse observational data and the complexities of representing deep-ocean dynamics. Future  
384 efforts should focus on enhancing observational data coverage and refining assimilation techniques for  
385 these challenging areas. To further improve the system's capabilities, plans are underway to assimilate  
386 more satellite-based ocean observations into the WCODA system. Furthermore, expanding the  
387 application of the WCODA system to other components of the climate model, such as the atmosphere  
388 and sea ice, could enhance overall predictive skill. These developments are essential for providing more  
389 accurate and reliable long-term climate predictions, ultimately aiding in the formulation of energy-sector  
390 policies and management strategies.

391

392 *Code and data availability.* The E3SMv2 code is publicly available under an open-source license through  
393 the Zenodo repository at <https://zenodo.org/records/13259801>. The EN4.2.1 monthly ocean temperature  
394 and salinity data are provided by the Met Office Hadley Centre via



395 <https://www.metoffice.gov.uk/hadobs/en4/>. The model data generated and analyzed during this study can  
396 be accessed on Zenodo at <https://zenodo.org/records/13283117>.

397

398 *Author contributions.* PS and LRL designed the experiments. PS developed the ocean assimilation code  
399 and conducted the experiments. BW proposed technical advice. PS and LRL analyzed the data. PS and  
400 LRL drafted the paper. All authors contributed to the revisions.

401

402 *Competing interests.* The authors declare no competing interests.

403

404 *Acknowledgements.* This research was supported by the Office of Science, U.S. Department of Energy  
405 Biological and Environmental Research through the Water Cycle and Climate Extremes Modeling  
406 (WACCEM) scientific focus area funded by the Regional and Global Model Analysis program area. This  
407 research used computing resources of the National Energy Research Scientific Computing Center, which  
408 is supported by the Office of Science of the U.S. Department of Energy under Contract No. DE-AC02-  
409 05CH1123, and BER Earth and Environmental System Modeling program's Compy computing cluster  
410 located at Pacific Northwest National Laboratory. Pacific Northwest National Laboratory is operated by  
411 Battelle Memorial Institute for the U.S. Department of Energy under contract DE-AC05-76RL01830.



412 **References**

- 413 Armour, K. C., Marshall, J., Scott, J. R., Donohoe, A., and Newsom, E. R.: Southern Ocean warming  
414 delayed by circumpolar upwelling and equatorward transport, *Nature Geoscience*, 9(7), 549–554,  
415 <https://doi.org/10.1038/ngeo2731>, 2016.
- 416 Balmaseda, M. A., Trenberth, K. E., & Källén, E.: Distinctive climate signals in reanalysis of global ocean  
417 heat content, *Geophysical Research Letters*, 40, 1754–1759, <https://doi.org/10.1002/grl.50382>, 2013.
- 418 Branstator, G., and Teng, H.: Potential impact of initialization on decadal predictions as assessed for  
419 CMIP5 models, *Geophysical Research Letters*, 39, L12703, <https://doi.org/10.1029/2012GL051974>,  
420 2012.
- 421 Browne, P. A., De Rosnay, P., Zuo, H., Bennett, A., and Dawson, A.: Weakly coupled ocean–atmosphere  
422 data assimilation in the ECMWF NWP system, *Remote Sensing*, 11, 234,  
423 <https://doi.org/10.3390/rs11030234>, 2019.
- 424 Carrasi, A., Bocquet, M., Bertino, L., and Evensen, G.: Data assimilation in the geosciences: An  
425 overview of methods, issues, and perspectives, *Wiley Interdisciplinary Reviews: Climate Change*, 9,  
426 e535, <https://doi.org/10.1002/wcc.535>, 2018.
- 427 Chen, J., Liu, H., Bai, C., Yan, H., Lu, K., Bao, S., and Liu, K.: Identifying climate modes contributing to  
428 sea surface salinity decadal variation in the North Pacific Ocean, *Journal of Geophysical Research:*  
429 *Oceans*, 125(10), e2019JC016011, <https://doi.org/10.1029/2019JC016011>, 2020.
- 430 Craig, A. P., Vertenstein, M., and Jacob, R.: A new flexible coupler for Earth system modeling developed  
431 for CCSM4 and CESM1, *International Journal of High Performance Computing Applications*, 26(1),  
432 31–42, <https://doi.org/10.1177/1094342011428141>, 2012.
- 433 Dirmeyer, P. A., Halder, S., and Bombardi, R.: On the harvest of predictability from land states in a global  
434 forecast model, *Journal of Geophysical Research: Atmospheres*, 123, 111–127,  
435 <https://doi.org/10.1029/2018JD029103>, 2018.
- 436 Edwards, C. A., Moore, A. M., Hoteit, I., and Cornuelle, B. D.: Regional ocean data assimilation, *Annual*  
437 *Review of Marine Science*, 7(1), 21–42, <https://doi.org/10.1146/annurev-marine-010814-015821>,  
438 2015.
- 439 Golaz, J. C., Caldwell, P. M., Van Roekel, L. P., Petersen, M. R., Tang, Q., Wolfe, J. D., Abeshu, G.,



440 Anantharaj, V., Asay-Davis, X. S., Bader, D. C., Baldwin, S. A., Bisht, G., Bogenschutz, P. A.,  
441 Branstetter, M., Brunke, M. A., Brus, S. R., Burrows, S. M., Cameron-Smith, P. J., Donahue, A. S.,  
442 Deakin, M., Easter, R. C., Evans, K. J., Feng, Y., Flanner, M., Foucar, J. G., Fyke, J. G., Griffin, B.  
443 M., Hannay, C., Harrop, B. E., Hoffman, M. J., Hunke, E. C., Jacob, R. L., Jacobsen, D. W., Jeffery,  
444 N., Jones, P. W., Keen, N. D., Klein, S. A., Larson, V. E., Leung, L. R., Li, H. Y., Lin, W., Lipscomb,  
445 W. H., Ma, P. L., Mahajan, S., Maltrud, M. E., Mametjanov, A., McClean, J. L., McCoy, R. B., Neale,  
446 R. B., Price, S. F., Qian, Y., Rasch, P. J., Reeves Eyre, J. E. J., Riley, W. J., Ringler, T. D., Roberts,  
447 A. F., Roesler, E. L., Salinger, A. G., Shaheen, Z., Shi, X., Singh, B., Tang, J., Taylor, M. A., Thornton,  
448 P. E., Turner, A. K., Veneziani, M., Wan, H., Wang, H., Wang, S., Williams, D. N., Wolfram, P. J.,  
449 Worley, P. H., Xie, S., Yang, Y., Yoon, J.-H., Zelinka, M. D., Zender, C. S., Zeng, X., Zhang, C.,  
450 Zhang, K., Zhang, Y., Zheng, X., Zhou, T., and Zhu, Q.: The DOE E3SM Coupled Model Version 1:  
451 Overview and Evaluation at Standard Resolution, *Journal of Advances in Modeling Earth Systems*,  
452 11, 2089–2129, <https://doi.org/https://doi.org/10.1029/2018MS001603>, 2019.

453 Golaz, J. C., Van Roekel, L. P., Zheng, X., Roberts, A. F., Wolfe, J. D., Lin, W. Y., Bradley, A. M., Tang,  
454 Q., Maltrud, M. E., Forsyth, R. M., Zhang, C. Z., Zhou, T., Zhang, K., Zender, C. S., Wu, M. X.,  
455 Wang, H. L., Turner, A. K., Singh, B., Richter, J. H., Qin, Y., Petersen, M. R., Mametjanov, A., Ma,  
456 P., Larson, V. E., Krishna, J., Keen, N. D., Jeffery, N., Hunke, E. C., Hannah, W. M., Guba, O.,  
457 Griffin, B. M., Feng, Y., Engwirda, D., Vittorio, A. V., Cheng, D., Conlon, L. M., Chen, C., Brunke,  
458 M. A., Bisht, G., Benedict, J. J., Asay-Davis, X. S., Zhang, Y. Y., Zhang, M., Zeng, X. B., Xie, S. C.,  
459 Wolfram, P. J., Vo, T., Veneziani, M., Tesfa, T. K., Sreepathi, S., Salinger, A. G., Jack Reeves Eyre,  
460 J. E., Prather, M. J., Mahajan, S., Li, Q., Jones, P. W., Jacob, R. L., Huebler, G. W., Huang, X. L.,  
461 Hillman, B. R., Harrop, B. E., Foucar, J. G., Fang, Y. L., Comeau, D. S., Caldwell, P. M., Bartoletti,  
462 T., Balaguru, K., Taylor, M. A., McCoy, R. B., Leung, L. R., and Bader, D. C.: The DOE E3SM  
463 Model version 2: Overview of the physical model and initial model evaluation, *Journal of Advances  
464 in Modeling Earth Systems*, 14, e2022MS003156, <https://doi.org/10.1029/2022MS003156>, 2022.

465 Good, S. A., Martin, M. J., and Rayner, N. A.: EN4: Quality controlled ocean temperature and salinity  
466 profiles and monthly objective analyses with uncertainty estimates, *Journal of Geophysical Research:  
467 Oceans*, 118(12), 6704–6716, <https://doi.org/10.1002/2013JC009067>, 2013.



- 468 Guo, Y., Yu, Y., Lin, P., Liu, H., He, B., Bao, Q., Zhao, S. and Wang, X.: Overview of the CMIP6 historical  
469 experiment datasets with the climate system model CAS FGOALS-f3-L, *Advances in Atmospheric*  
470 *Sciences*, 37, 1057–1066, <https://doi.org/10.1007/s00376-020-2004-4>, 2020.
- 471 He, Y., Wang, B., Liu, M., Liu, L., Yu, Y., Liu, J., Li, R., Zhang, C., Xu, S., Huang, W., Liu, Q., Wang,  
472 Y., and Li, F.: Reduction of initial shock in decadal predictions using a new initialization strategy,  
473 *Geophysical Research Letters*, 44(16), 8538–8547, <https://doi.org/10.1002/2017GL074028>, 2017.
- 474 He, Y., Wang, B., Liu, L., Huang, W., Xu, S., Liu, J., Wang, Y., Li, L., Huang, X., Peng, Y., Lin, Y., and  
475 Yu, Y.: A DRP-4DVar-based coupled data assimilation system with a simplified off-line localization  
476 technique for decadal predictions, *Journal of Advances in Modeling Earth Systems*, 12(4),  
477 e2019MS001768, <https://doi.org/10.1029/2019MS001768>, 2020.
- 478 Higgins, R. W., Leetmaa, A., Xue, Y., and Barnston, A.: Dominant factors influencing the seasonal  
479 predictability of US precipitation and surface air temperature, *Journal of Climate*, 13(22), 3994–  
480 4017, [https://doi.org/10.1175/1520-0442\(2000\)013<3994:DFITSP>2.0.CO;2](https://doi.org/10.1175/1520-0442(2000)013<3994:DFITSP>2.0.CO;2), 2000.
- 481 Jacobs, G., D’Addezio, J. M., Ngodock, H., and Souopgui, I.: Observation and model resolution  
482 implications to ocean prediction, *Ocean Modelling*, 159, 101760,  
483 <https://doi.org/10.1016/j.ocemod.2021.101760>, 2021.
- 484 Laloyaux, P., Balmaseda, M., Dee, D., Mogensen, K., and Janssen, P.: A coupled data assimilation system  
485 for climate reanalysis, *Quarterly Journal of the Royal Meteorological Society*, 142, 65–78,  
486 <https://doi.org/10.1002/qj.2629>, 2016.
- 487 Leung, L. R., Bader, D. C., Taylor, M. A., and McCoy, R. B.: An introduction to the E3SM special  
488 collection: Goals, science drivers, development, and analysis, *Journal of Advances in Modeling*  
489 *Earth Systems*, 12(11), e2019MS001821, <https://doi.org/10.1029/2019MS001821>, 2020.
- 490 Li, F., Wang, B., He, Y., Huang, W., Xu, S., Liu, L., Liu, J. and Li, L.: Important role of North Atlantic  
491 air–sea coupling in the interannual predictability of summer precipitation over the eastern Tibetan  
492 Plateau, *Climate Dynamics*, 56, 1433–1448, <https://doi.org/10.1007/s00382-020-05542-6>, 2021.
- 493 Li, H. Y., Wigmosta, M. S., Wu, H., Huang, M., Ke, Y., Coleman, A. M., and Leung, L. R.: A physically  
494 based runoff routing model for land surface and Earth system models, *Journal of Hydrometeorology*,  
495 14, 808–828, <https://doi.org/10.1175/JHM-D-12-015.1>, 2013.



- 496 McPhaden, M. J., Zebiak, S. E., and Glantz, M. H.: ENSO as an integrating concept in earth science,  
497 Science, 314, 1740–1745, <https://doi.org/10.1126/science.1132588>, 2006.
- 498 Penny, S. G., and Hamill, T. M.: Coupled data assimilation for integrated earth system analysis and  
499 prediction, Bulletin of the American Meteorological Society, 98, 169–172,  
500 <https://doi.org/10.1175/BAMS-D-17-0036.1>, 2017.
- 501 Pohlmann, H., Müller, W. A., Bittner, M., Hettrich, S., Modali, K., Pankatz, K., and Marotzke, J.:  
502 Realistic quasi-biennial oscillation variability in historical and decadal hindcast simulations using  
503 CMIP6 forcing, Geophysical Research Letters, 46(23), 14118–14125,  
504 <https://doi.org/10.1029/2019GL084878>, 2019.
- 505 Polkova, I., Köhl, A., and Stammer, D.: Climate-mode initialization for decadal climate predictions,  
506 Climate Dynamics, 53(11), 7097–7111, <https://doi.org/10.1007/s00382-019-04975-y>, 2019.
- 507 Reckinger, S. M., Petersen, M. R., and Reckinger, S. J.: A study of overflow simulations using MPAS-  
508 Ocean: Vertical grids, resolution, and viscosity, Ocean Modeling, 96, 291–313,  
509 <https://doi.org/10.1016/j.ocemod.2015.09.006>, 2015.
- 510 Ropelewski, C. F., and Halpert, M. S.: North American precipitation and temperature patterns associated  
511 with the El Niño/Southern Oscillation (ENSO), Monthly Weather Review, 114, 2352–2362,  
512 [https://doi.org/10.1175/1520-0493\(1986\)114<2352:NAPATP>2.0.CO;2](https://doi.org/10.1175/1520-0493(1986)114<2352:NAPATP>2.0.CO;2), 1986.
- 513 Shi, P., Wang, B., He, Y., Lu, H., Yang, K., Xu, S. M., Huang, W. Y., Liu, L., Liu, J. J., Li, L. J., and Wang,  
514 Y.: Contributions of weakly coupled data assimilation-based land initialization to interannual  
515 predictability of summer climate over Europe, Journal of Climate, 35, 517–535,  
516 <https://doi.org/10.1175/JCLI-D-20-0506.1>, 2022.
- 517 Shi, P., Lu, H., Leung, L.R., He, Y., Wang, B., Yang, K., Yu, L., Liu, L., Huang, W., Xu, S., Liu, J., Huang,  
518 X., Li, L., and Lin, Y.: Significant land contributions to interannual predictability of East Asian  
519 summer monsoon rainfall, Earth's Future, 9(2), e2020EF001762,  
520 <https://doi.org/10.1029/2020EF001762>, 2021.
- 521 Shi, P., Leung, L. R., Wang, B., Zhang, K., Hagos, S. M., and Zhang, S.: The 4DEnVar-based weakly  
522 coupled land data assimilation system for E3SM version 2, Geoscientific Model Development, 17,  
523 3025–3040, <https://doi.org/10.5194/gmd-17-3025-2024>, 2024.





- 524 Sluka, T. C., Penny, S. G., Kalnay, E., and Miyoshi, T.: Assimilating atmospheric observations into the  
525 ocean using strongly coupled ensemble data assimilation, *Geophysical Research Letters*, 43, 752–  
526 759, <https://doi.org/10.1002/2015GL067238>, 2016.
- 527 Smith, P. J., Fowler, A. M., and Lawless, A. S.: Exploring strategies for coupled 4D-Var data assimilation  
528 using an idealised atmosphere–ocean model, *Tellus A: Dynamic Meteorology and Oceanography*,  
529 67, 27025, <https://doi.org/10.3402/tellusa.v67.27025>, 2015.
- 530 Stammer, D., Balmaseda, M., Heimbach, P., Köhl, A., and Weaver, A.: Ocean data assimilation in support  
531 of climate applications: Status and perspectives, *Annual Review of Marine Science*, 8(1), 491–518,  
532 <https://doi.org/10.1146/annurev-marine-122414-034113>, 2016.
- 533 Tardif, R., Hakim, G. J., and Snyder, C.: Coupled atmosphere–ocean data assimilation experiments with  
534 a low-order climate model, *Climate Dynamics*, 43, 1631–1643, <https://doi.org/10.1007/s00382-013-1989-0>, 2014.
- 536 Taylor, M. A., Guba, O., Steyer, A., Ullrich, P. A., Hall, D. M., and Eldred, C.: An energy consistent  
537 discretization of the nonhydrostatic equations in primitive variables, *Journal of Advances in*  
538 *Modeling Earth Systems*, 12, e2019MS001783, <https://doi.org/10.1029/2019MS001783>, 2020.
- 539 Tian, T., Yang, S., Karami, M. P., Massonnet, F., Kruschke, T., and Koenigk, T.: Benefits of sea ice  
540 initialization for the interannual-to-decadal climate prediction skill in the Arctic in EC-Earth3,  
541 *Geoscientific Model Development*, 14, 4283–4305, <https://doi.org/10.5194/gmd-14-4283-2021>,  
542 2021.
- 543 Turner, A. K., Lipscomb, W. H., Hunke, E. C., Jeffery, N., Engwirda, D., Ringler, T. D., and Wolfe, J. D.:  
544 MPAS-Seaice (v1.0.0): Sea-ice dynamics on unstructured Voronoi meshes, *Geoscientific Model*  
545 *Development*, 15, 3721–3751, <https://doi.org/10.5194/gmd-15-3721-2022>, 2022.
- 546 Wang, B., Liu, J., Wang, S., Cheng, W., Liu, J., Liu, C., Xiao, Q., and Kuo, Y. H.: An economical approach  
547 to four-dimensional variational data assimilation, *Advances in Atmospheric Sciences*, 27, 715–727,  
548 <https://doi.org/10.1007/s00376-009-9122-3>, 2010.
- 549 Wang, B., Liu, J., Liu, L., Xu, S., and Huang, W.: An approach to localization for ensemble-based data  
550 assimilation, *PloS one*, 13(1), e0191088, <https://doi.org/10.1371/journal.pone.0191088>, 2018.
- 551 Wang, T., Geyer, W. R., Engel, P., Jiang, W., and Feng, S.: Mechanisms of tidal oscillatory salt transport



552 in a partially stratified estuary, *Journal of Physical Oceanography*, 45(11), 2773–2789,  
553 <https://doi.org/10.1175/JPO-D-15-0031.1>, 2015.

554 Wunsch, C., & Heimbach, P.: Practical global oceanic state estimation, *Physica D: Nonlinear Phenomena*,  
555 230, 197–208, <https://doi.org/10.1016/j.physd.2006.09.040>, 2007.

556 Yao, J., Vitart, F., Balmaseda, M. A., Wu, T., and Liu, X.: The impact of coupled data assimilation on  
557 Madden–Julian Oscillation predictability initialized from coupled satellite-era reanalysis, *Monthly*  
558 *Weather Review*, 149, 2897–2912, <https://doi.org/10.1175/MWR-D-20-0360.1>, 2021.

559 Yeager, S., Karspeck, A., Danabasoglu, G., Tribbia, J., and Teng, H.: A decadal prediction case study:  
560 Late twentieth-century North Atlantic Ocean heat content, *Journal of Climate*, 25, 5173–5189,  
561 <https://doi.org/10.1175/JCLI-D-11-00595.1>, 2012.

562 Yoshida, T., and Kalnay, E.: Correlation-cutoff method for covariance localization in strongly coupled  
563 data assimilation, *Monthly Weather Review*, 146, 2881–2889, [https://doi.org/10.1175/MWR-D-17-](https://doi.org/10.1175/MWR-D-17-0365.1)  
564 0365.1, 2018.

565 Zhang, M., Xie, S., Liu, X., Zhang, D., Lin, W., Zhang, K., Golaz, J. C., Zheng, X., and Zhang, Y.:  
566 Evaluating EAMv2 Simulated High Latitude Clouds Using ARM Measurements in the Northern and  
567 Southern Hemispheres, *Journal of Geophysical Research: Atmospheres*, 128(15), e2022JD038364,  
568 <https://doi.org/10.1029/2022JD038364>, 2023.

569 Zhang, S., Harrison, M. J., Wittenberg, A. T., Rosati, A., Anderson, J. L., and Balaji, V.: Initialization of  
570 an ENSO forecast system using a parallelized ensemble filter, *Monthly Weather Review*, 133, 3176–  
571 3201, <https://doi.org/10.1175/MWR3024.1>, 2005.

572 Zhang, S., Chang, Y. S., Yang, X., and Rosati, A.: Balanced and coherent climate estimation by combining  
573 data with a biased coupled model, *Journal of Climate*, 27, 1302–1314, [https://doi.org/10.1175/JCLI-](https://doi.org/10.1175/JCLI-D-13-00260.1)  
574 D-13-00260.1, 2014.

575 Zhang, S., Liu, Z., Zhang, X., Wu, X., Han, G., Zhao, Y., Yu, X., Liu, C., Liu, Y., Wu, S., Lu, F., Li, M.,  
576 Deng, X.: Coupled data assimilation and parameter estimation in coupled ocean–atmosphere models:  
577 a review, *Climate Dynamics*, 54, 5127–5144, <https://doi.org/10.1007/s00382-020-05275-6>, 2020.

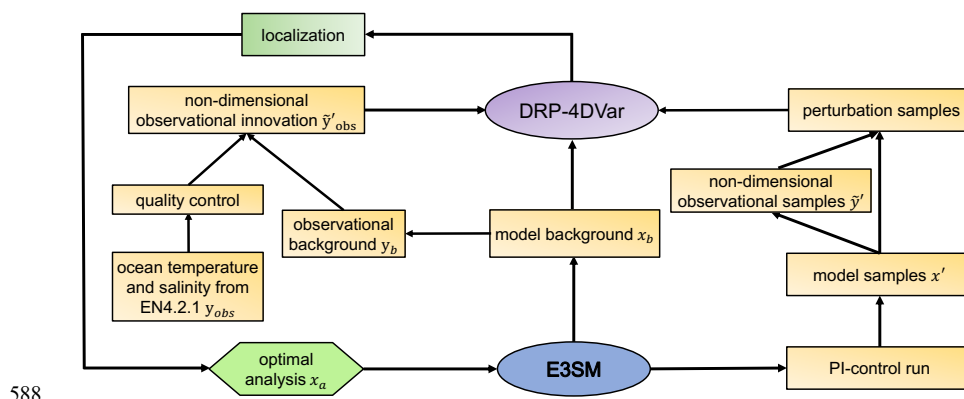
578 Zhao, Y., Wang, B., and Liu, J.: A DRP–4DVar data assimilation scheme for typhoon initialization using  
579 sea level pressure data, *Monthly weather review*, 140(4), 1191–1203, [22](https://doi.org/10.1175/MWR-</a></p></div><div data-bbox=)



580 D-10-05030.1, 2012.

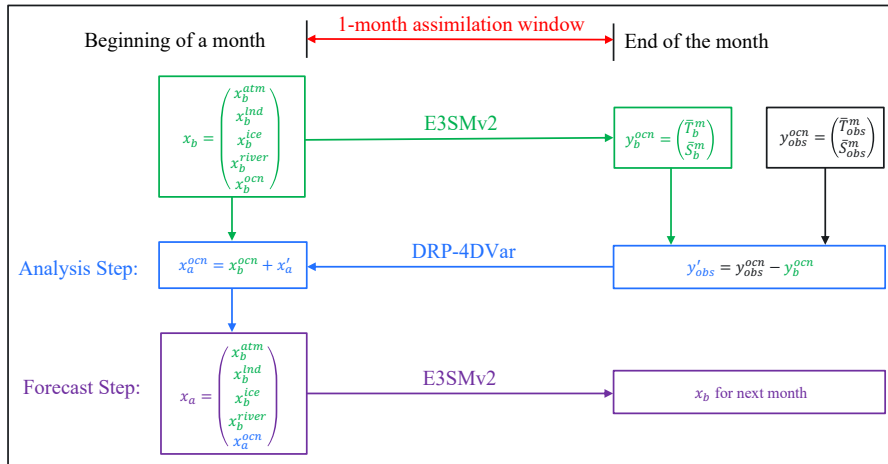
581 Zhou, W., Li, J., Yan, Z., Shen, Z., Wu, B., Wang, B., Zhang, R., and Li, Z.: Progress and future prospects  
582 of decadal prediction and data assimilation: a review, Atmospheric and Oceanic Science Letters, 17,  
583 100441, <https://doi.org/10.1016/j.aosl.2023.100441>, 2024.

584 Zhu, S., Wang, B., Zhang, L., Liu, J., Liu, Y., Gong, J., Xu, S., Wang, Y., Huang, W., Liu, L., He, Y., and  
585 Wu, X.: A Four-Dimensional Ensemble-Variational (4DEnVar) Data Assimilation System Based on  
586 GRAPES-GFS: System Description and Primary Tests, Journal of Advances in Modeling Earth  
587 Systems, 14(7), e2021MS002737, <https://doi.org/10.1029/2021MS002737>, 2022.



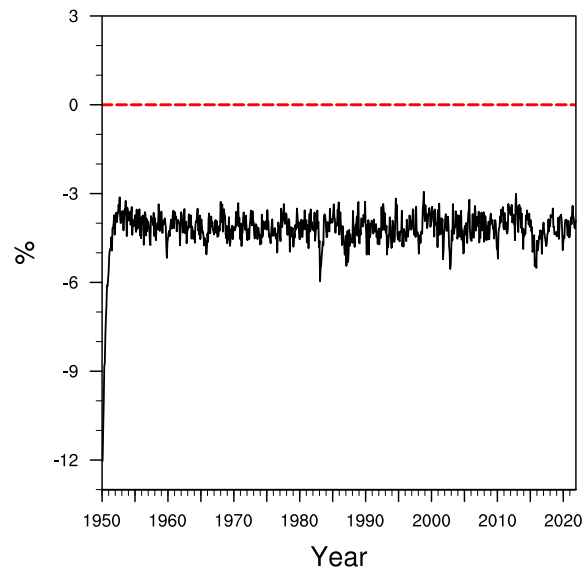
588

589 **Figure 1.** Workflow of the 4DVar-based WCODA system utilizing the DRP-4DVar method for the  
590 E3SM model (modified from Fig. 1 in Shi et al. (2024)).



591

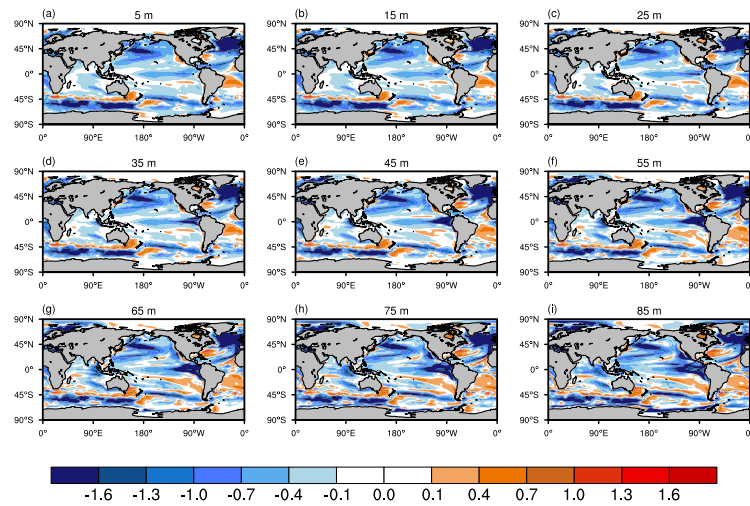
592 **Figure 2.** Schematic diagram of the DRP-4DVar assimilation process within the 4DEnVar-based  
 593 WCODA system for E3SM. The model background ( $x_b$ ) includes atmospheric ( $x_b^{atm}$ ), land ( $x_b^{lnd}$ ), ice  
 594 ( $x_b^{ice}$ ), river ( $x_b^{river}$ ), and oceanic ( $x_b^{ocn}$ ) components of the fully coupled E3SMv2. The observational  
 595 background ( $y_b^{ocn}$ ) is defined by the model outputs of monthly mean ocean temperature ( $\bar{T}_b^m$ ) and salinity  
 596 ( $\bar{S}_b^m$ ) using  $x_b$  as the initial state. The ocean observation ( $y_{obs}^{ocn}$ ) represents the observed monthly mean  
 597 ocean temperature ( $\bar{T}_{obs}^m$ ) and salinity ( $\bar{S}_{obs}^m$ ) from the EN4.2.1 reanalysis. The observational innovation  
 598 ( $y'_{obs}$ ) is calculated as the difference between the observed ocean temperature and salinity ( $y_{obs}^{ocn}$ ) and the  
 599 model's observational background ( $y_b^{ocn}$ ).  $x'_a$  denotes the analysis increment. The optimal analysis ( $x_a$ )  
 600 encompasses both the optimal analysis of the ocean component ( $x_a^{ocn}$ ) and the background states of other  
 601 components. This optimal analysis ( $x_a$ ) is used as the initial condition to produce the next month's  
 602 forecast, transferring ocean reanalysis information to other components.



603

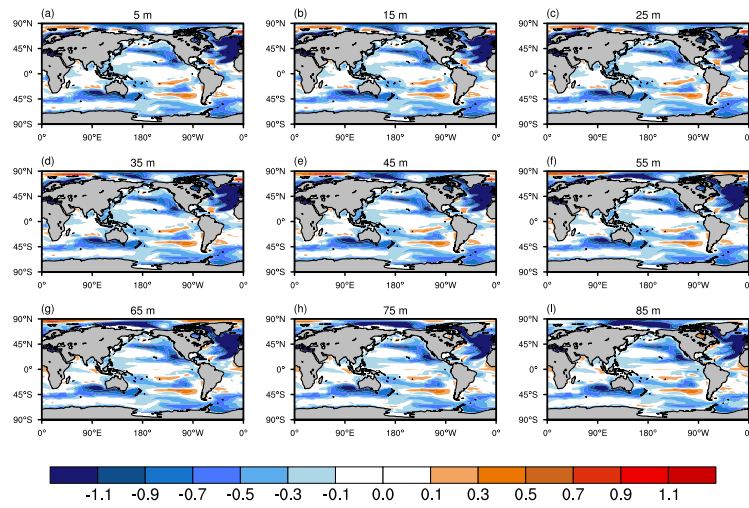
604 **Figure 3.** Temporal variation of the cost function reduction in the WCODA system based on the 4DEnVar

605 method from 1950 to 2021.



606

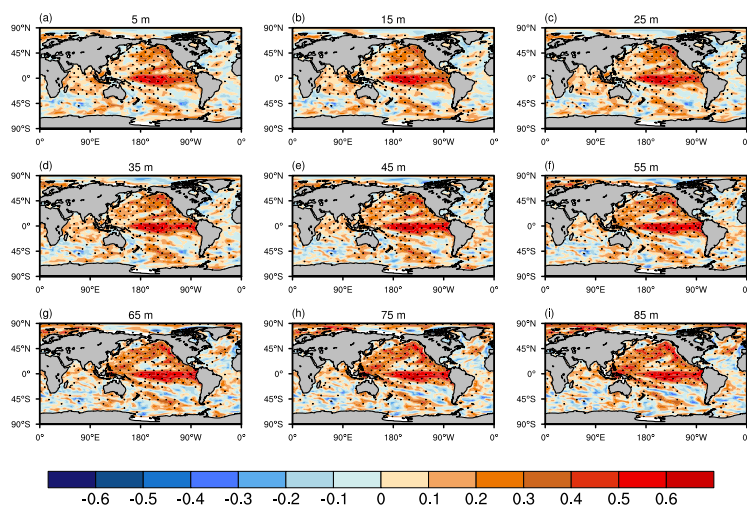
607 **Figure 4.** Spatial patterns of the root mean square error (RMSE) differences in ocean temperature  
608 between ASSIM and CTRL across nine ocean layers from 1950 to 2021. The RMSE differences are  
609 shown for nine different ocean depths: (a) 5 m, (b) 15 m, (c) 25 m, (d) 35 m, (e) 45 m, (f) 55 m, (g) 65  
610 m, (h) 75 m, and (i) 85 m.



611

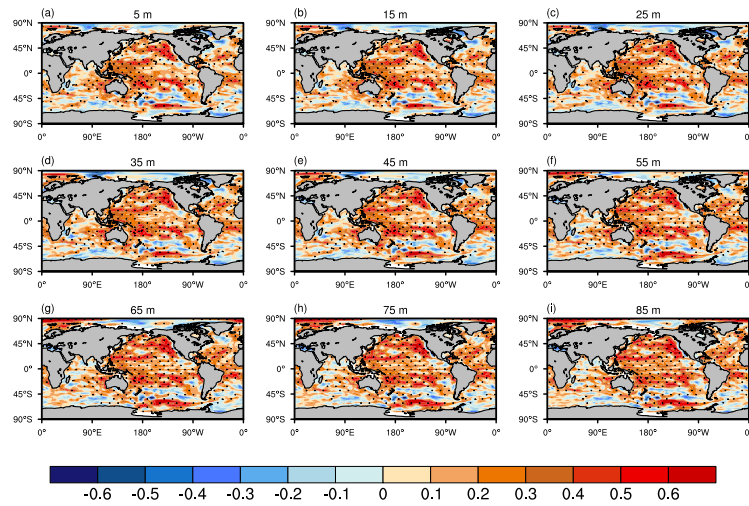
612 **Figure 5.** Similar to Figure 4 but for ocean salinity.





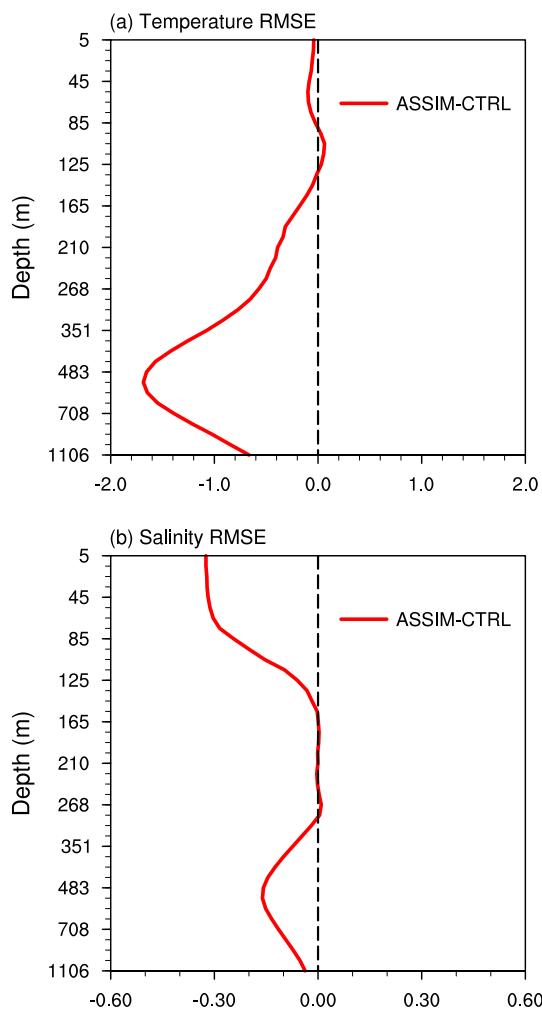
613

614 **Figure 6.** Spatial patterns of the differences between ASSIM and CTRL for their correlations of ocean  
615 temperature with observations across nine ocean layers for the period 1950-2021. Regions with stippling  
616 indicate statistical significance at the 95% confidence level. Panels (a) to (i) represent different ocean  
617 depths: (a) 5 m, (b) 15 m, (c) 25 m, (d) 35 m, (e) 45 m, (f) 55 m, (g) 65 m, (h) 75 m, and (i) 85 m.



618

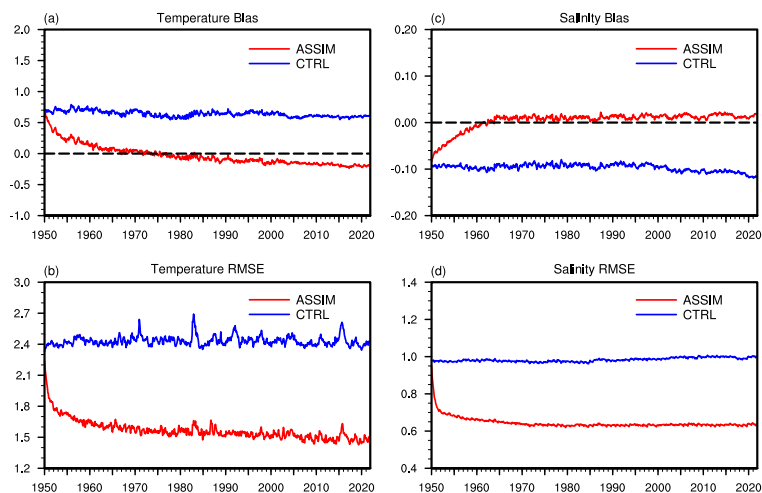
619 **Figure 7.** Similar to Figure 6 but for ocean salinity.



620

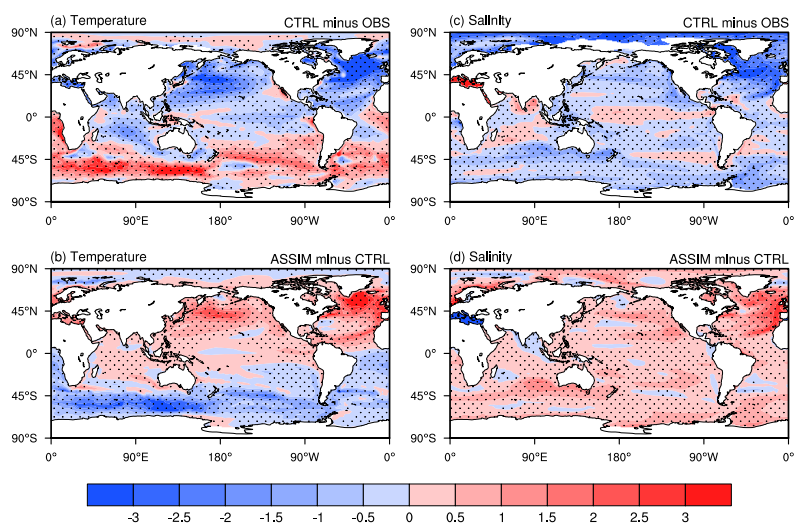
621 **Figure 8.** Vertical profiles of the globally averaged RMSE differences between ASSIM and CTRL for

622 (a) ocean temperature and (b) ocean salinity over the period from 1950 to 2021.



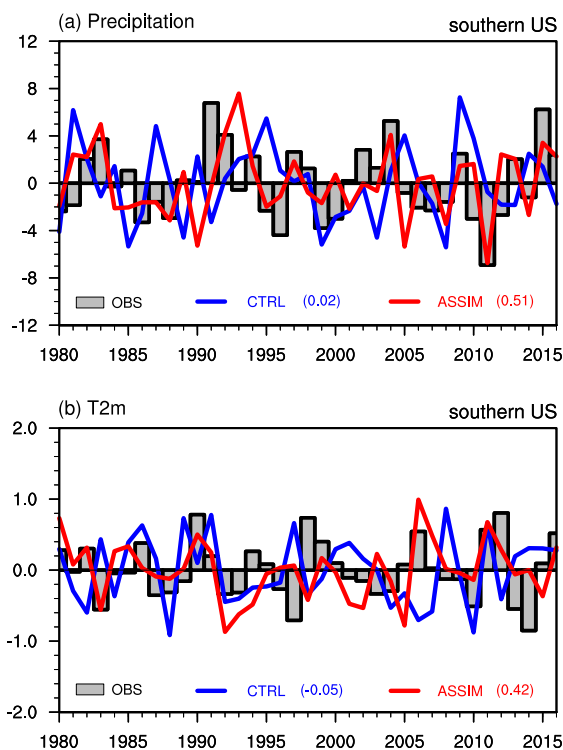
623

624 **Figure 9.** Temporal variations of bias (a, c) and RMSE (b, d) for the global mean ocean temperature and  
625 salinity averaged over the top 1000 meters from 1950 to 2021. The red lines represent ASSIM, while the  
626 blue lines represent CTRL.



627

628 **Figure 10.** Climatological mean differences in sea surface temperature (left) and salinity (right) from  
629 1950 to 2021. The top panels show the differences between CTRL and observation, while the bottom  
630 panels show the differences between ASSIM and CTRL. Dotted areas indicate regions where the  
631 differences are statistically significant at the 95% confidence level.



632  
633 **Figure 11.** Time series of interannual (a) precipitation and (b) surface air temperature anomalies in the  
634 southern US (24°-36°N, 105°-75°W). Gray bar: observation; blue line: CTRL; red line: ASSIM.  
635 Correlation coefficients of CTRL and ASSIM with observations are also shown. Both precipitation and  
636 temperature anomalies are computed after removing the climatology and its long-term trend from 1980  
637 to 2016. The observed precipitation and temperature are sourced from the GPCP precipitation data and  
638 ERA5 reanalysis, respectively.